

## Article

# A Facile Synthesis of P(VDF-TrFE)-Coated-PMMA Janus Membranes for Guided Bone Regeneration

Qin Luo, Xuzhao He, Xiyue Duan, Haoqing Liu, Zhiyuan Zhou and Kui Cheng \*

Center of Rehabilitation Biomedical Materials, State Key Laboratory of Silicon Materials, School of Materials Science and Engineering, Zhejiang University, Hangzhou 310027, China

\* Correspondence: chengkui@zju.edu.cn

**Abstract:** Bone repair and regeneration have aroused widespread interest due to their potential usefulness in cases when bone self-healing is insufficient. In this work, a Poly(vinylidene fluoride-trifluoroethylene)-coated-Poly methyl methacrylate Janus membrane was prepared, where a P(VDF-TrFE) coating on a PMMA film serves as Janus-A to mediate cell growth behavior, owing to its electroactivity, and the PMMA film serves as Janus-B to inhibit soft-tissue growth. A P(VDF-TrFE) coating separated from the substrate was put above the PMMA film before the PMMA film had dried completely, and a Janus membrane formed because of the flowability and adhesion of the nonvolatile PMMA solution. Their bonding could withstand the pressure of the body fluids in the shear direction. Various crystallization substrates were also applied to modulate the P(VDF-TrFE) coating's surface potentials, as the surface potential would further affect cellular response. It was also found that the responses of the bone marrow mesenchymal stem cells (BMSCs) and bone marrow macrophages (BMDMs) could be adjusted through surface potential modification. Such a Janus membrane could potentially be applied to a biological environment with the effect of both guiding bone regeneration and preventing soft tissue adhesion.



**Citation:** Luo, Q.; He, X.; Duan, X.; Liu, H.; Zhou, Z.; Cheng, K. A Facile Synthesis of P(VDF-TrFE)-Coated-PMMA Janus Membranes for Guided Bone Regeneration. *Coatings* **2022**, *12*, 1947. <https://doi.org/10.3390/coatings12121947>

Academic Editor: Jun-Beom Park

Received: 17 October 2022

Accepted: 7 December 2022

Published: 11 December 2022

**Publisher's Note:** MDPI stays neutral with regard to jurisdictional claims in published maps and institutional affiliations.



**Copyright:** © 2022 by the authors. Licensee MDPI, Basel, Switzerland. This article is an open access article distributed under the terms and conditions of the Creative Commons Attribution (CC BY) license (<https://creativecommons.org/licenses/by/4.0/>).

**Keywords:** Janus membrane; P(VDF-TrFE); PMMA; bone tissue regeneration

## 1. Introduction

Bone diseases such as bone infections and bone loss require bone tissue regeneration, yet bone self-healing is insufficient owing to numerous pathological conditions. External intervention is desired to promote bone repair [1–3]. Guided bone regeneration (GBR) developed into a therapy in the 1980s [4,5] and has been applied to heal bone defects [6], even reaching the level of the reconstruction of new bone and the treatment of bone deficiency [7]. GBR is a technology whereby a specific membrane is put above the area of the bone defect to reduce the cell adhesion from other tissue [8]. In the healing process, various kinds of cells migrate at different speeds into the bone defect area. A GBR membrane could cover the bone defect area and create a mechanical barrier to exclude the migration of cells that impede bone regeneration (for example, fibroblasts) and provide space to encourage bone regeneration [9]. GBR membranes usually fulfill the requests of biocompatibility and excluding action [10,11]. Dahlin et al. [12] applied an expanded Polytetrafluoroethylene membrane to cover the bone defect area in the mandibular angle and found that the membrane could reduce the degree of tissue adhesion and promote bone healing. Lekovic et al. [13] validated that a membrane consisting of Poly(vinyl alcohol) and polylactic acid could protect the alveolar bone and prevent bone defects in the alveolar ridge area.

Nevertheless, the barrier membrane is usually short of bioactivity and the capability to contribute to new bone tissue formation [14]. Some strategies have been adapted to facilitate the proliferation and migration of bone cells and achieve rapid bone tissue formation. Ma et al. [15] reported that they prepared a novel asymmetric collagen/chitosan

GBR membrane, and that the membrane ultimately promoted osteoblasts' growth in an *in vitro* experiment. Almansoori et al. [16] loaded poly(caprolactone) and  $\beta$ -tricalcium phosphate scaffolds with mesenchymal stem cells and platelet-rich plasma, and the bone regeneration capacity was boosted in the end. However, the method of directly doping osteogenic factor into membranes is limited by the release period and speed [17].

The concept of Janus has also been applied to invent advanced biomedical devices [18]. A Janus membrane has diversified properties on each side in a broad sense, such as the component, surface potential, wettability, and so on [19]. Wang et al. [17] designed gelatin (GEL) nanofibers loaded with hydroxyapatite as an inlayer to promote osteoconductivity; meanwhile, the outer layer was made of poly(caprolactone) (PCL) nanofibers for mechanical strength. Yang et al. developed an adhesive Janus periosteum with a topographical surface on one side for bone regeneration and a natural periosteum on the other side [20]. In their study, the Janus definition was employed to fabricate a Poly(vinylidene fluoride-trifluoroethylene)-coated-Poly methyl methacrylate (P(VDF-TrFE)-coated-PMMA) Janus membrane, and the Janus membrane could guide bone repair and guard against the unnecessary adhesion of soft tissue. It is worth noting that Poly(vinylidene fluoride) (PVDF) is widely used due to its larger ferroelectricity response as well as its cytocompatibility [21,22]. After polarization through a high-voltage electric field, both the oriented arrangement of the electric dipole and positive or negative surface potentials are obtained easily [23]. The regulation of the crystallization behavior of PVDF, the electrical polarization field voltage, and the duration are all connected to the arrangement of the electric dipoles and the PVDF surface potential. The charged PVDF surface has been indicated to modulate cell behavior by dominating the interaction between the surface and the cells, determining, for instance, the conformation of the adsorbed proteins and altering the cell membrane potential [24]. Tang et al. [25] selected a  $\text{CoFe}_2\text{O}_4$ /P(VDF-TrFE) nanocomposite film and explored its role in cellular osteogenic differentiation, demonstrating that an obvious surface potential variation could control the conformation of adsorbed proteins and further influence the binding of integrin-adsorbed proteins. Szewczyk et al. [26] controlled the surface charge of PVDF fibers and indicated that the surface charge could lead the calcium channels of the cell to open and promote bone tissue regeneration. Poly methyl methacrylate (PMMA) processes low biological toxicity, and its bioactivity is as low as the main ingredient of bone cement [27,28].

In this work, P(VDF-TrFE)-coated-PMMA Janus membranes were prepared, where a P(VDF-TrFE) coating on a PMMA film served as Janus-A to mediate cell growth behavior owing to its electroactivity and the PMMA film served as Janus-B to inhibit soft-tissue growth. The interfacial charge of graphene/n-Si (Gr/n-Si) was applied to regulate the P(VDF-TrFE) crystallization in order to obtain diversified electrical properties. Various P(VDF-TrFE) coatings were applied to investigate their influence on the cell culture. The mechanical properties of the Janus membrane were also noted to ensure its supportability and the tight connection of Janus-A and Janus-B.

## 2. Materials and Methods

### 2.1. Materials

Monolayer graphene was bought from Nanjing Xianfeng Nanometer Material Technology Co. Ltd., and n-Si wafer (<100> orientation) with a single side polished was obtained from Gandy New Material Co. Ltd. (Suzhou, China). The polylactide (PLA) powders were manufactured by Changchun Sino-Biomaterials Co. Ltd. (Changchun, China). The P(VDF-TrFE) (70/30) powders used to prepare Janus-A were acquired from Piezotech (Paris, France), and the PMMA solid particles with a molecular weight of about 80,000~200,000 powders used to prepare Janus-B were purchased from Aladdin Chemical Reagent (Shanghai, China). The Polytetrafluoroethylene (PTFE) substrate was supplied by Taxun Co. Ltd. (Shenzhen, China). Dichloromethane, absolute ethanol, and acetone were gained from Sinopharm Chemical Reagent Co. Ltd. (Shanghai, China), and they were all of the analytical grades.

## 2.2. Sample Preparation

### 2.2.1. Preparation of P(VDF-TrFE) Coatings

The n-Si substrates were first ultrasonically preoxidized in acetone, absolute ethanol, and ultrapure water for about 30 min, and next immersed in a hydrofluoric acid (HF) aqueous solution for 5 min. Monolayer graphene was transferred to the n-Si substrate according to a previous paper [29]. In brief, monolayer graphene grown on copper was spin-coated with a PLA solution, and there was a supporting layer on graphene when the copper was etched by a  $(\text{NH}_4)_2\text{S}_2\text{O}_8$  solution. The monolayer graphene was transferred to the n-Si substrate, and the PLA layer was removed with dichloromethane eventually. A certain amount of P(VDF-TrFE) powders were added to acetone and subjected to 2 h of mechanical agitation to obtain a completely dissolved solution (0.1 g/mL). Subsequently, the P(VDF-TrFE)/acetone solution was spin-coated on the n-Si and graphene/n-Si substrates, and P(VDF-TrFE) coatings were formed after heat treating, where the treating temperature was 180 °C and the treating duration was 5 min. The electroactive P(VDF-TrFE) coatings were electrically polarized with an external electric field (2.5 kV) for 3 min and next washed with absolute ethanol and ultrapure water. The separation of the P(VDF-TrFE) coatings and the substrate was achieved by immersing the samples in ultrapure water because there was no chemical bond between the P(VDF-TrFE) coatings and smooth substrates.

### 2.2.2. Preparation of PMMA Film and Janus Membranes

Certain amounts of PMMA powders were added to acetone and subjected to 4 h of mechanical agitation to obtain a completely dissolved 0.2 g/mL solution. Next, the PMMA/acetone solution was spin-coated on a PTFE substrate. A P(VDF-TrFE) coating was put above the PMMA film before the PMMA film dried completely. In this process, they formed nice adhesion owing to the flowability of the nonvolatile PMMA solution. Eventually, the Janus structure was shaped and separated from the low-viscosity PTFE easily.

## 2.3. Characterization of Janus Membranes

The surface morphologies of the P(VDF-TrFE) coatings, the PMMA film, and a cross-section of the Janus membrane were observed by a field emission scanning electron microscope (FE-SEM, Hitachi SU-70, Tokyo, Japan) with a 3.0 kV acceleration voltage and an 8.0 mm depth of field. The crystal phase structure of the P(VDF-TrFE) coatings was analyzed using an X-ray diffractometer (PANalytical X'Pert PRO, Almelo, The Netherlands), where the lamp source was a Cu  $K\alpha$  radiation source at 30 kV and the scan rate was  $2^\circ \text{ min}^{-1}$  for the range of 15–50°. An infrared spectrometer (Nicolet 5700, Thermo Fisher Scientific, Waltham, MA, USA) was used to estimate the FTIR spectrum of the P(VDF-TrFE) coatings and PMMA film at a range of 600–4000  $\text{cm}^{-1}$ , and attenuation total reflection (ATR) technology was utilized in this process at room temperature. The ferroelectric hysteresis loops of the P(VDF-TrFE) coatings were measured with an RT66A ferroelectric tester Radiant Technologies Inc., Albuquerque, NM, USA). A quasi-state piezoelectric coefficient ( $d_{33}$ ) instrument (ZJ-3AN, Institute of Acoustics, Chinese Academy of Science, Beijing, China) was used to analyze the piezoelectric performance of the P(VDF-TrFE) coatings. The analysis of the spring constant in the vertical direction was achieved by using atomic force microscopy (AFM, NTEGRA Spectra, NT-MDT, Moscow, Russia) force-distance curves with the “contact” mode [30]. The surface potentials of the P(VDF-TrFE) coatings recrystallized on various substrates were observed by SKPM (NTEGRA Spectra, NT-MDT, Moscow, Russia). The shear bonding strength of P(VDF-TrFE) coating and the PMMA film was determined by a material testing machine (Instron 5943, Instron, Norwood, MA, USA). In this measuring process, the two sides of Janus membrane were agglutinated, respectively, by the upper and lower ends of the testing machine, and then the two ends moved in opposite directions. Finally, the composite was destructed and the load was recorded [31].

#### 2.4. Cell Culture

NIH3T3 cells (Chinese National Infrastructure of Cell Line Resource, with source number 1101MOU-PUMC000018) were cultured in Dulbecco's modified eagle medium (DMEM) containing 10% fetal bovine serum (Cellmax, Beijing, China) in a humid atmosphere (37 °C, 5% CO<sub>2</sub>). In addition, 1% MEM nonessential amino acids, 1% sodium pyruvate, 10 000 µg mL<sup>-1</sup> streptomycin, 1% antibiotic solution containing 10,000 units mL<sup>-1</sup> of penicillin (all from Gibco, Thermo Fisher Scientific, Waltham, MA, USA) were also supplemented into the medium. The NIH3T3 is a serial passage cell line with high contact inhibition established from NIH Swiss mouse embryos, where "3T3" refers to the cell transfer and inoculation protocol for the line, and means "3-day transfer, inoculum 3 \* 10<sup>5</sup> cells", and the cell line is subjected to more than 5 additional rounds of subcloning to make it more suitable for transformation analysis. Before we used NIH3T3 in this work, NIH3T3 experienced subculture 3 times, and the fourth-generation NIH3T3 was cultured in samples.

The bone marrow mesenchymal stem cells (BMSCs) were extracted from 3-week-old male Sprague Dawley rats and cultured in Dulbecco's modified eagle medium (DMEM, Cellmax, Beijing, China) with a low glucose type, containing 10% fetal bovine serum, in a humid atmosphere (37 °C, 5% CO<sub>2</sub>). Additionally, 1% MEM nonessential amino acids, 1% sodium pyruvate, 10,000 µg mL<sup>-1</sup> of streptomycin, and 1% antibiotic solution containing 10,000 units mL<sup>-1</sup> penicillin (all from Gibco, Thermo Fisher Scientific, Waltham, MA, USA) were supplemented into the medium.

The bone marrow cells were extracted from the femurs and tibias of 6-week-old C57 black mice [22]. Next, the cells were cultured in  $\alpha$  medium containing 10% fetal bovine serum (Cellmax, Beijing, China), 10,000 µg mL<sup>-1</sup> of streptomycin, and 1% antibiotic solution containing 10,000 units mL<sup>-1</sup> of penicillin (all from Gibco, Thermo Fisher Scientific, Waltham, MA, USA) in a humid atmosphere (37 °C, 5% CO<sub>2</sub>), and 30 pg µL<sup>-1</sup> of M-CSF was used to induce cells to differentiate to bone marrow macrophages (BMDMs).

All animal experiments were carried out under the approval of the Animal Experimental Ethical Committee of the First Affiliated Hospital, Zhejiang University School of Medicine.

#### 2.5. Cell Viability Assays

A 500 µL suspension of NIH3T3 cells (1 \* 10<sup>5</sup> cells mL<sup>-1</sup>) was inoculated on the surface of the P(VDF-TrFE) coating and PMMA film separately, and cultured for 1 and 3 days to compare the cell growth behavior (cell viability) on each side of the Janus membrane.

A 500 µL BMSCs suspension (1 \* 10<sup>5</sup> cells mL<sup>-1</sup>) was inoculated on the surfaces of the P(VDF-TrFE) coatings crystallized on different substrates, and cultured for 1 and 3 days to observe the cell viability on P(VDF-TrFE) coatings with different surface potentials.

The measure of the cell viability mentioned above was taken with the cell counting kit-8 (CCK-8, Dojindo Laboratories, Kumamoto, Japan). In brief, 550 µL of the mixed reagent containing the CCK-8 reagent and fresh cell culture medium (ratio of 1:10) was added, and the absorbance at 450 nm was measured by a microplate reader (Tecan, Infinite F50, Männedorf, Switzerland) after being kept in an incubator for 2 h.

#### 2.6. ALP Assay

For osteogenic differentiation, the alkaline phosphatase (ALP) content is a remarkable measuring standard. The 500 µL BMSCs suspension (1 \* 10<sup>5</sup> cells mL<sup>-1</sup>) was inoculated on the P(VDF-TrFE) coatings with various surface potentials and cultured for 7 and 14 days. When the culture finished, the cell lysate was collected, and then the ALP quantity and the total protein content were separately analyzed with both the LabAssay ALP (Wako, Japan) and the BCA protein assay kits (Thermo Fisher Scientific, Waltham, MA, USA) to determine the ALP activity of the total protein.

### 2.7. Immunofluorescence Staining

The 500  $\mu\text{L}$  BMSCs suspension ( $2 \times 10^4$  cells  $\text{mL}^{-1}$ ) was inoculated on the surfaces of P(VDF-TrFE) coatings with various surface potentials and cultured for 3 days, after which the nuclei and F-actin were stained with DAPI (Sigma, Ronkonkoma, NY, America) and Alexa-Fluor 594 phalloidin (Sigma), respectively.

The 500  $\mu\text{L}$  BMDMs suspension ( $2 \times 10^5$  cells  $\text{mL}^{-1}$ ) was inoculated on the surfaces of P(VDF-TrFE) coatings with various surface potentials and cultured for 3 days. The BMDMs were further incubated with primary antibodies (including rabbit anti-mouse iNOS and mouse anti-mouse CD206) and secondary antibodies (including donkey anti-rabbit Alexa Fluor-555 and goat anti-mouse Alexa Fluor-488) to assess the cell marker expression. DAPI was also employed to stain the nuclei for counterstaining cells.

Eventually, a confocal laser scanning microscope (CLSM, ZEISS LSM780, Oberkochen, Germany) was used to observe the MSCs morphologies and the BMDMs surface markers, and the related data were analyzed with ImageJ software.

### 2.8. Statistical Analysis

The statistical analysis was completed successfully by using Product and Service Solutions (SPSS) software (IBM SPSS Statistics 22, New York, NY, USA). A one-way analysis of variance (ANOVA) with post-hoc Scheffe test was applied to perform the statistical analysis. Dunnett's T3 test was utilized when the variance was inhomogeneous. Statistical significance exists when \*  $p < 0.05$ , \*\*  $p < 0.01$ , and \*\*\*  $p < 0.001$ . All data were represented as mean  $\pm$  standard deviation.

## 3. Results and Discussion

### 3.1. Characterization of Janus Membranes

As shown in Figure 1a, the combination of the P(VDF-TrFE) coating and PMMA film is tight, and there are no excess voids or cracks at the interface, which is due to the features of the PMMA solution and the preparation method. The undried PMMA film maintains a certain viscosity, while the uncured liquid of the PMMA maintains a certain flowability. According to the preparation described above, the P(VDF-TrFE)-coated-PMMA Janus membrane was obtained. The PMMA film, when dried completely, has a relatively smooth surface (Figure 1b), and some scientific research [32,33] indicates that a lower roughness often means a relatively more negative cellular response. To modulate the surface potential of the P(VDF-TrFE) coating, different recrystallization methods were employed. When the P(VDF-TrFE) coating was recrystallized on the Gr/n-Si substrate, 450 nm light ( $150 \text{ mW}/\text{cm}^2$ ) was exerted during the heating and cooling processes, and the P(VDF-TrFE) coating was named "PVDF-G1". Similarly, the P(VDF-TrFE) coating recrystallized on the Gr/n-Si substrate without light illumination was named "PVDF-G2". The morphologies of "PVDF-G1" (Figure 1c) and "PVDF-G2" (Figure 1d) present fibrous areas, which may be connected to the monolayer graphene. The monolayer graphene possesses an originally flat surface. According to the literature [34], the hexagon center-to-center distance of graphene is 2.460 nm, and the unit-cell parameter  $c$  of P(VDF-TrFE) is 2.55 nm. There is just a tiny mismatch. That allows van der Waals epitaxy of the P(VDF-TrFE) crystals, which could be the reason for the fibrillar morphologies. The P(VDF-TrFE) coating recrystallized on an n-Si substrate (PVDF-N1) possesses a relatively flat morphology, as shown in Figure 1e.

The X-ray diffraction (XRD) data for the P(VDF-TrFE) coatings are shown in Figure 1f, where the range including the obvious peak is chosen. The sharp peak at  $2\theta = 19.6^\circ$  relates to the (200) and (110) reflections of the  $\beta$ -phase [35]. The peak intensity and the full width at half maxima (FWHM) were measured, indicating that the P(VDF-TrFE) coatings mentioned above possess differentiated degrees of crystallization. The peak intensity value located at  $19.6^\circ$  of "PVDF-G1" is larger than the others, and the FWHM of "PVDF-G1" and "PVDF-G2" are approximate. According to the literature [36,37], the degree of crystallization is connected to intensity, and the degree of crystallization of the sample will decrease with the decreasing intensity of the main peak. Therefore, the degree of crystalliza-

tion of “PVDF-G1” is higher than that of the others because of the effect of the interfacial charge. The FTIR spectra of the P(VDF-TrFE) coatings are presented in Figure 1g. There are absorption bands of  $\beta$ -phase ( $840\text{ cm}^{-1}$  and  $1285\text{ cm}^{-1}$ ) and  $\gamma$ -phase ( $840\text{ cm}^{-1}$  and  $1245\text{ cm}^{-1}$ ) in the FTIR spectra [38], matching with the crystal structure components in the XRD data. The FTIR spectra of the PMMA film are presented in Figure 1h. The Spectrum exhibits typical bands for PMMA; for example, the absorptions at  $987\text{ cm}^{-1}$  and  $1453\text{ cm}^{-1}$  originate from O-CH<sub>3</sub> bending and stretching, and the bands at  $1250\text{ cm}^{-1}$  and  $1730\text{ cm}^{-1}$  could be ascribed to the stretching of the C=O groups, while a band  $1197\text{ cm}^{-1}$  can be ascribed to a C-O stretching vibration [39].

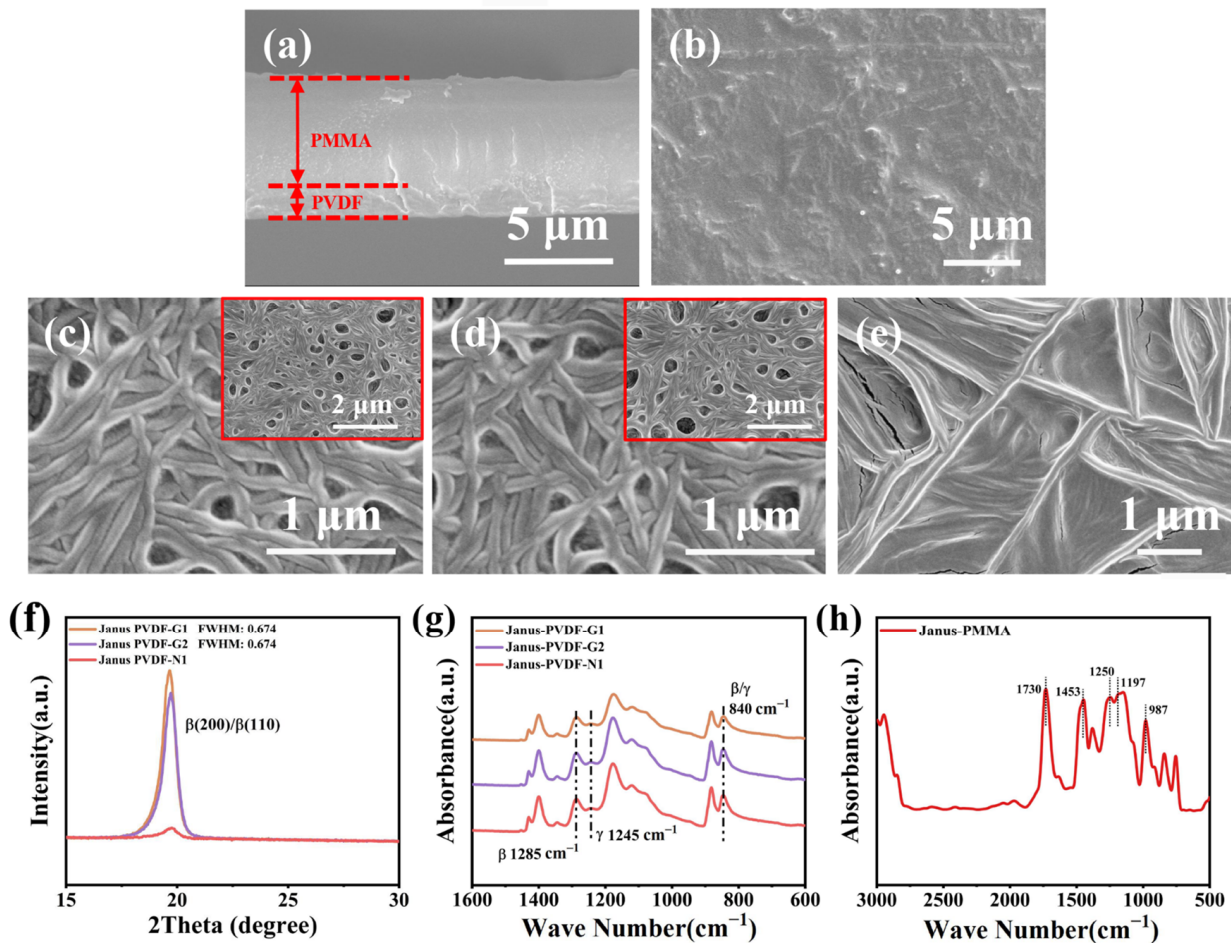


**Figure 1.** Cross-section image of Janus membrane (a), scanning electron microscope (SEM) images of PMMA film (b), P(VDF-TrFE) coating recrystallized on Gr/n-Si substrate with light illumination (c), P(VDF-TrFE) coating recrystallized on Gr/n-Si substrate without light illumination (d), P(VDF-TrFE) coating recrystallized on n-Si substrate (e). XRD patterns (f) and FTIR spectra (g,h) of P(VDF-TrFE) coatings and PMMA film.

### 3.2. Electrical and Mechanical Properties of Janus Membranes

The electricity of the P(VDF-TrFE) coating is associated with its degree of crystallization and the orientation of its dipoles. Figure 2a shows the ferroelectric polarization hysteresis loops of the P(VDF-TrFE) coatings by applying a 200 V test voltage. The “PVDF-G1” coating exhibits a better ferroelectric property than others. The “PVDF-G1” coating’s remnant polarization is  $0.0228\text{ }\mu\text{C cm}^{-2}$ , and its coercive field is 49.51 MV/m. The “PVDF-G2” coating’s remnant polarization of  $0.0114\text{ }\mu\text{C cm}^{-2}$  was also measured. As for the “PVDF-N1” coating, the ferroelectric polarization hysteresis loop presents a tight waist state, implying that the ferroelectricity of the “PVDF-N1” coating is inferior. With the same polarization voltage and period, the  $d_{33}$  are  $15.15 \pm 1.95\text{ pC/N}$ ,  $11.57 \pm 2.81\text{ pC/N}$ , and  $7.98 \pm 2.71\text{ pC/N}$ ,

respectively (Figure 2b), implying that there is also a certain difference in the  $d_{33}$  of the P(VDF-TrFE) coatings owing to the degrees of crystallization and ferroelectricity. The surface potentials of the P(VDF-TrFE) coatings after polarization were measured with SKPM, which intuitively exhibits the surface electric property. The surface potentials were found to be  $820.21 \pm 84.30$  mV (PVDF-G1),  $582.02 \pm 87.75$  mV (PVDF-G2), and  $394.40 \pm 11.03$  mV (PVDF-N2), which also indicates the adjustability of the P(VDF-TrFE) surface potential.

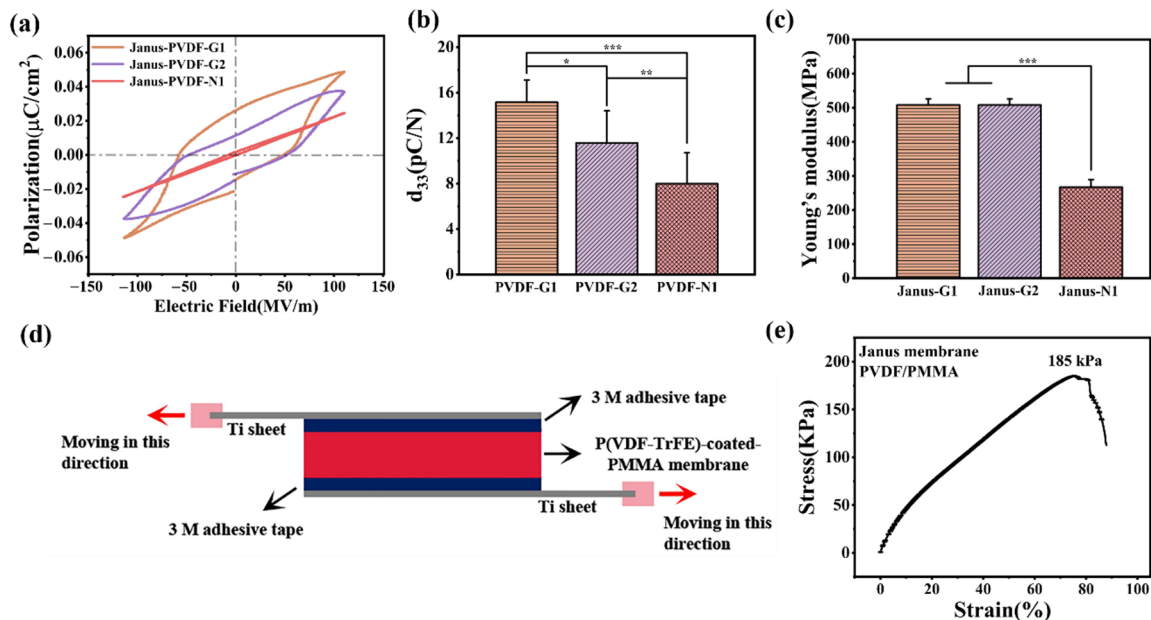


**Figure 2.** (a) Ferroelectric hysteresis loops of P(VDF-TrFE) coatings. (b) Piezoelectric coefficients ( $d_{33}$ ) of P(VDF-TrFE) coatings. (c) Spring constant of Janus membranes in the vertical direction. (d) Schematic diagram of shear bonding strength characterization. (e) Shear bonding strength of P(VDF-TrFE) coating and PMMA film (\*  $p < 0.05$ , \*\*  $p < 0.01$ , \*\*\*  $p < 0.001$ ).

When the Janus membrane is applied to an authentic biological environment, the mechanical properties of Janus also need to be taken into account. The spring constant in the vertical direction of Janus-G1 is  $525.72 \pm 26.99$  MPa, and the spring constant of Janus-G2 is  $508.17 \pm 18.11$  MPa. The values are both higher than Janus-N1 ( $266.96 \pm 22.76$  MPa). The results fit with the difference in the degree of crystallization, indicating that crystallization contributes to both electrical and mechanical properties. The shear bonding strength of the P(VDF-TrFE) coating and PMMA film is about 184.94 kPa, which means that the membrane could withstand the highest fluid pressure (8 kPa) in the shear direction [40]. When a tight bonding of the P(VDF-TrFE) coating and PMMA film is formed, the Janus membrane plays its role in the internal environment effectively.

### 3.3. Cellular Response on Janus Membranes

The cell growth behaviors on each side of the Janus membrane were also investigated. As shown in Figure 3, the P(VDF-TrFE) coating is more conducive to cell adhesion (1st day) and proliferation (3rd day) than the PMMA film, which proves that the PMMA film could inhibit soft tissue adhesion more effectively compared with P(VDF-TrFE) coating.

The implant's surface potential could induce the desired cell behavior, which originates from cellular characteristics such as ion channels and cell-surface receptor proteins [41,42]. The P(VDF-TrFE) coatings prepared on different substrates possess differentiated surface potentials. The influence of surface potential characteristics on cellular behaviors was also investigated. As shown in Figure 4a, the results indicate that PVDF-G1 could best enhance the viability of BMSCs compared to other coatings.

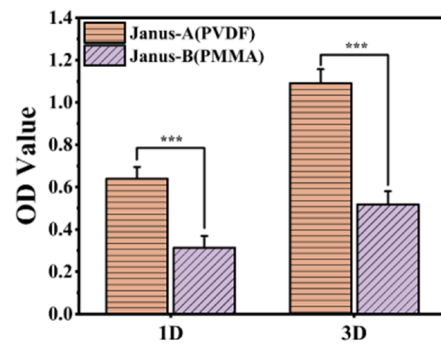


**Figure 3.** The adhesion (1 d) and proliferation (3 d) behaviors of NIH3T3 cells on P(VDF-TrFE) coating and PMMA film (\*\* $p < 0.001$ ).

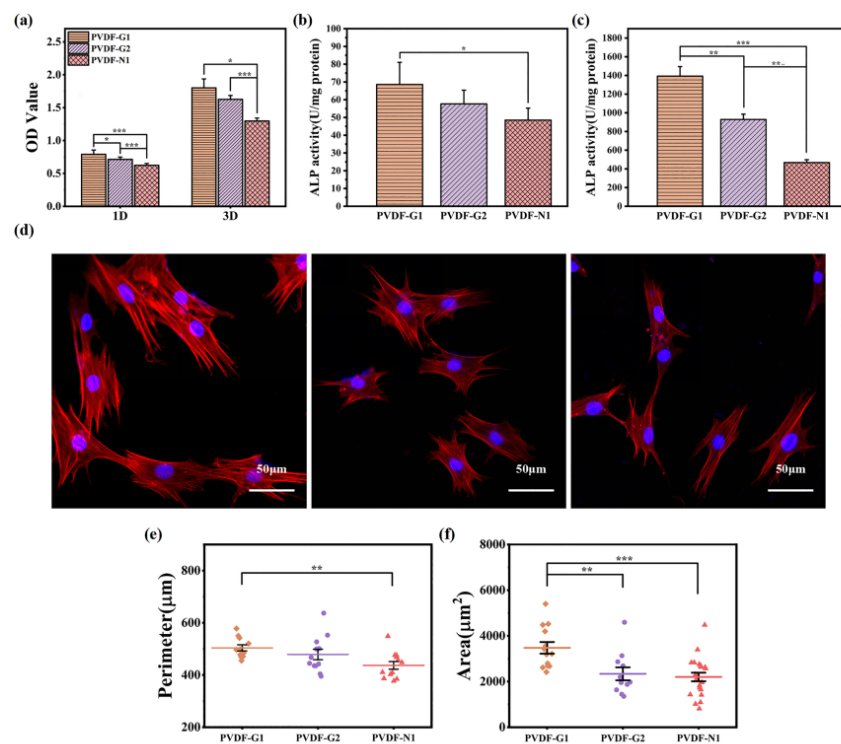


**Figure 4.** (a) The adhesion (1 d) and proliferation (3 d) behaviors of MSCs on P(VDF-TrFE) coating s. (b,c) ALP activities of MSCs on P(VDF-TrFE) coatings after culture for 7 days and 14 days. (d) The CLSM images of MSCs on P(VDF-TrFE) coatings for 3 days. (e,f) Cytomorphometric evaluations of MSCs on P(VDF-TrFE) coatings perimeter and spread area for 3 days (\*  $p < 0.05$ , \*\*  $p < 0.01$ , \*\*\*  $p < 0.001$ ).

The results in Figure 4b,c indicate that a higher surface potential elevates the response of the osteogenic differentiation of the BMSCs after 7-day and 14-day cultures, and the ALP expressions on the coatings all have significant improvements in the later cell growth period (14 days). As for the morphologies of the BMSCs after the 3-day culture (Figure 4d), there is an obvious difference in the perimeters and spread areas (Figure 4e,f). The BMSCs cultured on PVDF-G1 exhibits a larger spread area and perimeter than the others. The perimeter and spread area are associated with the growth and osteogenic differentiation of BMSCs, which is consistent with the experiment mentioned above. The appearances also indicate that the P(VDF-TrFE) coating's surface potential could be adjusted to regulate BMSCs behavior.

The process of bone tissue regeneration does not only depend on osteogenesis-related cells, as the immune response in tissue repair is also nonnegligible [43]. As they are a kind of heterogeneous immune cell, macrophages' surface marker expressions on the

P(VDF-TrFE) coatings with various surface potentials were also investigated. The marker could display the polarization state of macrophages visually [44]. In this work, iNOS and CD206 were chosen as the M1 and M2 phenotypic markers, respectively, where M1 refers to pro-inflammatory polarization and M2 refers to pro-healing polarization. According to the literature [45], the macrophages' switch from M1 to M2 tends to be associated with the formation of new bone owing to the release of osteogenic cytokines. The morphologies of macrophages (Figure 5a) and their polarization-related surface marker expression (Figure 5b) on the P(VDF-TrFE) coating with higher surface potential (PVDF-G1) show a significant improvement in the M2 phenotype compared with the M1 phenotype. Additionally, the expression of the M1 phenotype and the M2 phenotype are undifferentiated on PVDF-G2 and PVDF-N1, indicating that the inferior surface potential is unable to modulate cellular polarization behavior.

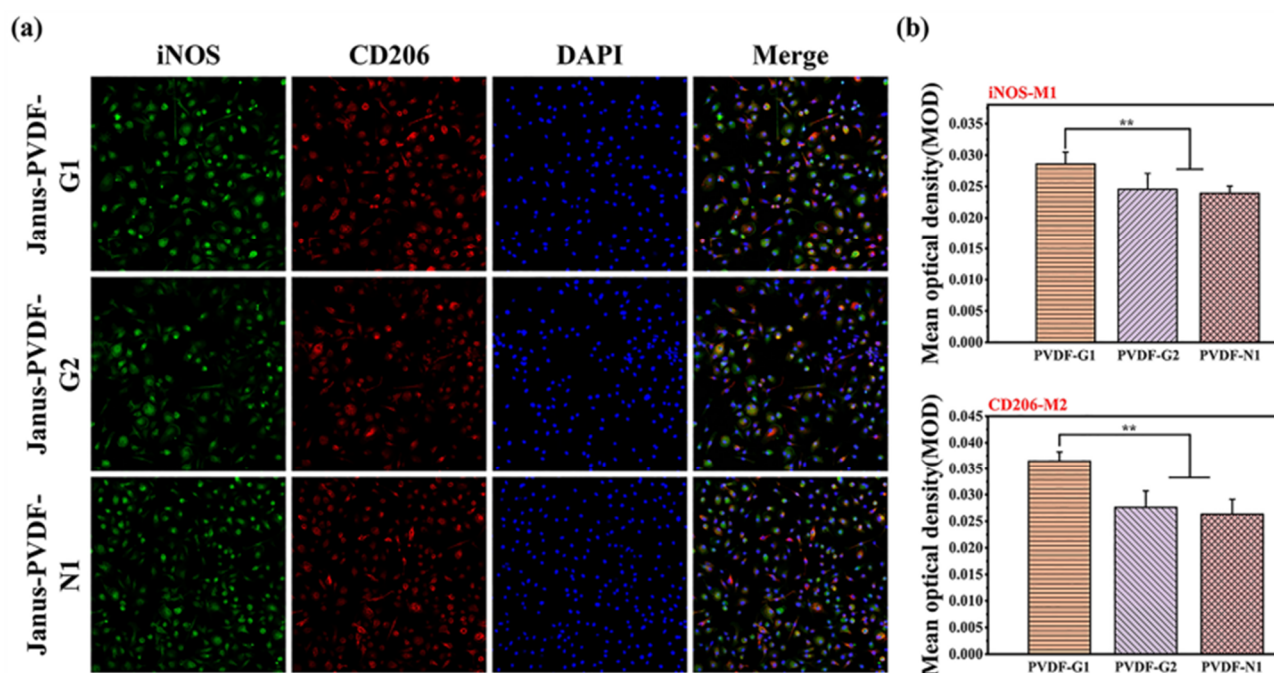


**Figure 5.** Immunofluorescence images (a) and semi-quantitative statistics (b) of the macrophage surface markers CD206 (M2 marker, red) and iNOS (M1 marker, green) (\*\*  $p < 0.01$ ).

#### 4. Conclusions

This study provides a method for preparing a P(VDF-TrFE)-coated-PMMA Janus membrane that possesses both anti-adhesion characteristics and characteristics that promote bone tissue adhesion. P(VDF-TrFE) coatings with various surface potentials were obtained by regulating the crystallization method. The mechanical properties and cellular response of the Janus membrane were also examined. The following points are concluded.

1. The P(VDF-TrFE) coatings and PMMA film were acquired with the spin-casting method, separately. Next, the P(VDF-TrFE) coating was put above the undried PMMA film to build the Janus membrane's structure. The tight bonding of the P(VDF-TrFE) coating and PMMA film could withstand the pressure of the body fluids in the shear direction.
2. The surfaces of the substrates could be used to adjust the crystallization behavior of the P(VDF-TrFE) coatings. As a result, the electrical properties and cellular responses could be controlled.
3. The P(VDF-TrFE) coatings could regulate the differentiation of the BMSCs and BMDMs responses through controllable surface potential, while the opposite PMMA side inhibits unnecessary NIH3T3 cell growth. That makes such Janus membranes a good alternate to GBR devices.

**Author Contributions:** Methodology, Q.L.; investigation, Q.L. and X.H.; data curation, Q.L. and X.D.; writing—original draft preparation, Q.L. and H.L.; visualization, Z.Z.; conceptualization, K.C. All authors have read and agreed to the published version of the manuscript.

**Funding:** This research was funded by National Key R&D Program of China (2021YFC2400400), the National Natural Science Foundation of China (Grant No. 51872259, 52072339, 51972284, 51902135) and the 111 Project (B16042).

**Institutional Review Board Statement:** Not applicable.

**Informed Consent Statement:** Not applicable.

**Data Availability Statement:** The authors confirm that the data supporting the findings of this study are available within the article.

**Conflicts of Interest:** The authors declare no conflict of interest.

## References

1. Bai, X.; Gao, M.; Syed, S.; Zhuang, J.; Xu, X.; Zhang, X.-Q. Bioactive hydrogels for bone regeneration. *Bioact. Mater.* **2018**, *3*, 401–417. [[CrossRef](#)] [[PubMed](#)]
2. Klein, G.L. Disruption of bone and skeletal muscle in severe burns. *Bone Res.* **2015**, *3*, 15002. [[CrossRef](#)] [[PubMed](#)]
3. Winkler, T.; Sass, F.A.; Duda, G.N.; Schmidt-Bleek, K. A review of biomaterials in bone defect healing, remaining shortcomings and future opportunities for bone tissue engineering: The unsolved challenge. *Bone Jt. Res.* **2018**, *7*, 232–243. [[CrossRef](#)] [[PubMed](#)]
4. Dahlin, C.; Linde, A.; Gottlow, J.; Nyman, S. Healing of Bone Defects by Guided Tissue Regeneration. *Plast. Reconstr. Surg.* **1988**, *81*, 672–676. [[CrossRef](#)]
5. Nyman, S.; Lindhe, J.; Karring, T.; Rylander, H. New attachment following surgical treatment of human periodontal disease. *J. Clin. Periodontol.* **1982**, *9*, 290–296. [[CrossRef](#)]
6. Karfeld-Sulzer, L.S.; Ghayor, C.; Siegenthaler, B.; Gjoksi, B.; Pohjonen, T.H.; Weber, F.E. Comparative study of NMP-preloaded and dip-loaded membranes for guided bone regeneration of rabbit cranial defects. *J. Tissue Eng. Regen. Med.* **2014**, *11*, 425–433. [[CrossRef](#)]
7. Elgali, I.; Omar, O.; Dahlin, C.; Thomsen, P. Guided bone regeneration: Materials and biological mechanisms revisited. *Eur. J. Oral Sci.* **2017**, *125*, 315–337. [[CrossRef](#)]
8. Park, K.O.; Lee, J.H.; Park, J.H.; Shin, Y.C.; Huh, J.B.; Bae, J.-H.; Kang, S.H.; Hong, S.W.; Kim, B.; Yang, D.J.; et al. Graphene oxide-coated guided bone regeneration membranes with enhanced osteogenesis: Spectroscopic analysis and animal study. *Appl. Spectrosc. Rev.* **2016**, *51*, 540–551. [[CrossRef](#)]
9. Fu, L.; Wang, Z.; Dong, S.; Cai, Y.; Ni, Y.; Zhang, T.; Wang, L.; Zhou, Y. Bilayer Poly(Lactic-co-glycolic acid)/Nano-Hydroxyapatite Membrane with Barrier Function and Osteogenesis Promotion for Guided Bone Regeneration. *Materials* **2017**, *10*, 257. [[CrossRef](#)]
10. Aprile, P.; Letourneur, D.; Simon-Yarza, T. Membranes for Guided Bone Regeneration: A Road from Bench to Bedside. *Adv. Health. Mater.* **2020**, *9*, 2000707. [[CrossRef](#)]
11. Lee, H.-S.; Byun, S.-H.; Cho, S.-W.; Yang, B.-E. Past, Present, and Future of Regeneration Therapy in Oral and Periodontal Tissue: A Review. *Appl. Sci.* **2019**, *9*, 1046. [[CrossRef](#)]
12. Dahlin, C.; Sennerby, L.; Lekholm, U.; Linde, A.; Nyman, S. Generation of new bone around titanium implants using a membrane technique: An experimental study in rabbits. *Int. J. Oral Maxillofac. Implant.* **1989**, *4*, 19–25.
13. Lekovic, V.; Camargo, P.M.; Klokkevold, P.R.; Weinlaender, M.; Kenney, E.B.; Dimitrijevic, B.; Nedic, M. Preservation of Alveolar Bone in Extraction Sockets Using Bioabsorbable Membranes. *J. Periodontol.* **1998**, *69*, 1044–1049. [[CrossRef](#)] [[PubMed](#)]
14. Pitaluga, L.H.; Souza, M.T.; Zanutto, E.D.; Romero, M.E.S.; Hatton, P.V. Electrospun F18 Bioactive Glass/PCL—Poly ( $\epsilon$ -caprolactone)—Membrane for Guided Tissue Regeneration. *Materials* **2018**, *11*, 400. [[CrossRef](#)] [[PubMed](#)]
15. Ma, S.; Adayi, A.; Liu, Z.; Li, M.; Wu, M.; Xiao, L.; Sun, Y.; Cai, Q.; Yang, X.; Zhang, X.; et al. Asymmetric Collagen/chitosan Membrane Containing Minocycline-loaded Chitosan Nanoparticles for Guided Bone Regeneration. *Sci. Rep.* **2016**, *6*, 31822. [[CrossRef](#)] [[PubMed](#)]
16. Almansoori, A.A.; Kwon, O.-J.; Nam, J.-H.; Seo, Y.-K.; Song, H.-R.; Lee, J.-H. Mesenchymal stem cells and platelet-rich plasma-impregnated polycaprolactone- $\beta$  tricalcium phosphate bio-scaffold enhanced bone regeneration around dental implants. *Int. J. Implant Dent.* **2021**, *7*, 35. [[CrossRef](#)]
17. Wang, Q.; Feng, Y.; He, M.; Zhao, W.; Qiu, L.; Zhao, C. A Hierarchical Janus Nanofibrous Membrane Combining Direct Osteogenesis and Osteoimmunomodulatory Functions for Advanced Bone Regeneration. *Adv. Funct. Mater.* **2021**, *31*, 2008906. [[CrossRef](#)]
18. Liang, W.; He, W.; Huang, R.; Tang, Y.; Li, S.; Zheng, B.; Lin, Y.; Lu, Y.; Wang, H.; Wu, D. Peritoneum-Inspired Janus Porous Hydrogel with Anti-Deformation, Anti-Adhesion, and Pro-Healing Characteristics for Abdominal Wall Defect Treatment. *Adv. Mater.* **2022**, *34*, 2108992. [[CrossRef](#)]
19. Yang, H.; Hou, J.; Chen, V.; Xu, Z. Janus Membranes: Exploring Duality for Advanced Separation. *Angew. Chem. Int. Ed.* **2016**, *55*, 13398–13407. [[CrossRef](#)]

20. Yang, Y.; Xu, T.; Bei, H.P.; Zhao, Y.; Zhao, X. Sculpting Bio-Inspired Surface Textures: An Adhesive Janus Periosteum. *Adv. Funct. Mater.* **2021**, *31*, 2104636. [[CrossRef](#)]
21. Zhang, J.; He, X.; Chen, X.; Wu, Y.; Dong, L.; Cheng, K.; Lin, J.; Wang, H.; Weng, W. Enhancing osteogenic differentiation of BMSCs on high magnetoelectric response films. *Mater. Sci. Eng. C* **2020**, *113*, 110970. [[CrossRef](#)] [[PubMed](#)]
22. Wang, Z.; He, X.; Tang, B.; Chen, X.; Dong, L.; Cheng, K.; Weng, W. Polarization behavior of bone marrow-derived macrophages on charged P(VDF-TrFE) coatings. *Biomater. Sci.* **2021**, *9*, 874–881. [[CrossRef](#)] [[PubMed](#)]
23. Jia, F.; Lin, S.; He, X.; Zhang, J.; Shen, S.; Wang, Z.; Tang, B.; Li, C.; Wu, Y.; Dong, L.; et al. Comprehensive Evaluation of Surface Potential Characteristics on Mesenchymal Stem Cells' Osteogenic Differentiation. *ACS Appl. Mater. Interfaces* **2019**, *11*, 22218–22227. [[CrossRef](#)] [[PubMed](#)]
24. Metwally, S.; Stachewicz, U. Surface potential and charges impact on cell responses on biomaterials interfaces for medical applications. *Mater. Sci. Eng. C* **2019**, *104*, 109883. [[CrossRef](#)]
25. Tang, B.; Zhuang, J.; Wang, L.; Zhang, B.; Lin, S.; Jia, F.; Dong, L.; Wang, Q.; Cheng, K.; Weng, W.-J. Harnessing Cell Dynamic Responses on Magnetolectric Nanocomposite Films to Promote Osteogenic Differentiation. *ACS Appl. Mater. Interfaces* **2018**, *10*, 7841–7851. [[CrossRef](#)]
26. Szewczyk, P.K.; Metwally, S.; Karbowniczek, J.E.; Marzec, M.M.; Stodolak-Zych, E.; Gruszczyński, A.; Bernasik, A.; Stachewicz, U. Surface-Potential-Controlled Cell Proliferation and Collagen Mineralization on Electrospun Polyvinylidene Fluoride (PVDF) Fiber Scaffolds for Bone Regeneration. *ACS Biomater. Sci. Eng.* **2019**, *5*, 582–593. [[CrossRef](#)]
27. Sabri, B.A.; Satgunam, M.; Abreeza, N.; Abed, A.N. A review on enhancements of PMMA Denture Base Material with Different Nano-Fillers. *Cogent Eng.* **2021**, *8*, 1875968. [[CrossRef](#)]
28. Pahlevanzadeh, F.; Bakhsheshi-Rad, H.; Ismail, A.; Aziz, M.; Chen, X.B. Development of PMMA-Mon-CNT bone cement with superior mechanical properties and favorable biological properties for use in bone-defect treatment. *Mater. Lett.* **2019**, *240*, 9–12. [[CrossRef](#)]
29. Long, X.; Wang, X.; Yao, L.; Lin, S.; Zhang, J.; Weng, W.; Cheng, K.; Wang, H.; Lin, J. Graphene/Si-Promoted Osteogenic Differentiation of BMSCs through Light Illumination. *ACS Appl. Mater. Interfaces* **2019**, *11*, 43857–43864. [[CrossRef](#)]
30. Cappella, B.; Dietler, G. Force-distance curves by atomic force microscopy. *Surf. Sci. Rep.* **1999**, *34*, 1–104. [[CrossRef](#)]
31. Cheng, Z.; Cheng, K.; Weng, W. SiO<sub>2</sub>/TiO<sub>2</sub> Nanocomposite Films on Polystyrene for Light-Induced Cell Detachment Application. *ACS Appl. Mater. Interfaces* **2017**, *9*, 2130–2137. [[CrossRef](#)] [[PubMed](#)]
32. Zhou, K.; Li, Y.; Zhang, L.; Jin, L.; Yuan, F.; Tan, J.; Yuan, G.; Pei, J. Nano-micrometer surface roughness gradients reveal topographical influences on differentiating responses of vascular cells on biodegradable magnesium. *Bioact. Mater.* **2021**, *6*, 262–272. [[CrossRef](#)] [[PubMed](#)]
33. Hu, X.; Mei, S.; Wang, F.; Qian, J.; Xie, D.; Zhao, J.; Yang, L.; Wu, Z.; Wei, J. Implantable PEKK/tantalum microparticles composite with improved surface performances for regulating cell behaviors, promoting bone formation and osseointegration. *Bioact. Mater.* **2020**, *6*, 928–940. [[CrossRef](#)] [[PubMed](#)]
34. Kim, K.L.; Lee, W.; Hwang, S.K.; Joo, S.H.; Cho, S.M.; Song, G.; Cho, S.H.; Jeong, B.; Hwang, I.; Ahn, J.-H.; et al. Epitaxial Growth of Thin Ferroelectric Polymer Films on Graphene Layer for Fully Transparent and Flexible Nonvolatile Memory. *Nano Lett.* **2016**, *16*, 334–340. [[CrossRef](#)]
35. Han, J.; Li, D.; Zhao, C.; Wang, X.; Li, J.; Wu, X. Highly Sensitive Impact Sensor Based on PVDF-TrFE/Nano-ZnO Composite Thin Film. *Sensors* **2019**, *19*, 830. [[CrossRef](#)]
36. Agarwal, U.P.; Ralph, S.A.; Reiner, R.S.; Baez, C. Probing crystallinity of never-dried wood cellulose with Raman spectroscopy. *Cellulose* **2016**, *23*, 125–144. [[CrossRef](#)]
37. Gaur, M.S.; Singh, P.K.; Ali, A.; Singh, R. Thermally stimulated discharge current (TSDC) characteristics in  $\beta$ -phase PVDF-BaTiO<sub>3</sub> nanocomposites. *J. Therm. Anal. Calorim.* **2014**, *117*, 1407–1417. [[CrossRef](#)]
38. Cai, X.; Lei, T.; Sun, D.; Lin, L. A critical analysis of the  $\alpha$ ,  $\beta$  and  $\gamma$  phases in poly(vinylidene fluoride) using FTIR. *RSC Adv.* **2017**, *7*, 15382–15389. [[CrossRef](#)]
39. Dukali, R.M.; Radović, I.M.; Stojanović, D.B.; Šević, D.D.; Radojević, V.J.; Jocić, D.M.; Aleksić, R.R. Electrospinning of laser dye Rhodamine B-doped poly(methyl methacrylate) nanofibers. *J. Serbian Chem. Soc.* **2014**, *79*, 867–880. [[CrossRef](#)]
40. Qin, Y.-X.; Kaplan, T.; Saldanha, A.; Rubin, C. Fluid pressure gradients, arising from oscillations in intramedullary pressure, is correlated with the formation of bone and inhibition of intracortical porosity. *J. Biomech.* **2003**, *36*, 1427–1437. [[CrossRef](#)]
41. Mycielska, M.E.; Djamgoz, M.B.A. Cellular mechanisms of direct-current electric field effects: Galvanotaxis and metastatic disease. *J. Cell Sci.* **2004**, *117*, 1631–1639. [[CrossRef](#)] [[PubMed](#)]
42. Hashimoto, M.; Kitaoka, S.; Furuya, M.; Kanetaka, H.; Hoshikaya, K.; Yamashita, H.; Abe, M. Enhancement of cell differentiation on a surface potential-controlled nitrogen-doped TiO<sub>2</sub> surface. *J. Ceram. Soc. Jpn.* **2019**, *127*, 636–641. [[CrossRef](#)]
43. Mori, G.; D'Amelio, P.; Faccio, R.; Brunetti, G. The Interplay between the Bone and the Immune System. *Clin. Dev. Immunol.* **2013**, *2013*, 720504. [[CrossRef](#)] [[PubMed](#)]
44. Schlundt, C.; Fischer, H.; Bucher, C.H.; Rendenbach, C.; Duda, G.N.; Schmidt-Bleek, K. The multifaceted roles of macrophages in bone regeneration: A story of polarization, activation and time. *Acta Biomater.* **2021**, *133*, 46–57. [[CrossRef](#)] [[PubMed](#)]
45. Zetao, C.; Travis, K.; Rachael, M.; Ross, C.; Jiang, C.; Chengtie, W.; Yin, X. Osteoimmunomodulation for the development of advanced bone biomaterials. *Mater. Today* **2016**, *19*, 304–321. [[CrossRef](#)]